Nuclear Engineering and Design 250 (2012) 520–537

Contents lists available at SciVerse ScienceDirect

Nuclear Engineering and Design

journal homepage: www.elsevier.com/locate/nucengdes

Experimental and numerical evaluation of debris transport augmentation by turbulence during the recirculation-cooling phase of a LOCA

Jong Pil Park[a], Kyung Sik Choi[a], Ji Hwan Jeong[a,*], Gyung Min Choi[a], Ju Yeop Park[b], Man Woong Kim[c]

[a] School of Mechanical Engineering, Pusan National University, Jangjeon-dong, Geumjeong-gu, Busan, Republic of Korea
[b] Korea Institute of Nuclear Safety, Guseong-dong, Yuseong-gu, Daejeon, Republic of Korea
[c] International Atomic Energy Agency, Wagramerstrasse 5, 1400 Vienna, Austria

HIGHLIGHTS

- The debris transport fraction during the recirculation phase after a LOCA.
- Evaluation w/and w/o consideration of turbulence.
- Experimental and numerical analysis were performed.
- Large increase in debris transport fraction when turbulence is considered.

ARTICLE INFO

Article history:
Received 28 July 2011
Received in revised form 10 May 2012
Accepted 25 May 2012

ABSTRACT

In resolving the safety issue of sump clogging due to debris generated by the type of high-energy line break known as a GSI-191 event, determination of the debris transport fraction, which is likely to be augmented by fluid turbulence during the recirculation cooling phase of a pressurized water reactor (PWR), is very important in the sizing of the sump screen area. In the present study, the debris transport fraction during the recirculation cooling phase of the OPR1000 plant is evaluated with and without consideration of turbulence debris augmentation. To do this, first a computational fluid dynamics (CFD) analysis of the flooded containment floor during the recirculation cooling phase is performed to obtain mean flow fields and the turbulence kinetic energy field assuming a double-ended guillotine break of a hot leg. Then, experiments involving tumbling velocities measurements of the surrogate debris for the OPR1000 plant and supplementary CFD analyses are performed to verify the turbulence effect on debris transport. From these findings, the turbulence effect on the degree of debris floor tumbling augmentation was found to be represented by the algebraic sum of the mean horizontal velocity and the horizontal fluctuating velocity deduced from the turbulent kinetic energy (TKE). Based on this experimental finding and on the CFD analysis of the containment floor when flooded, the debris transport fraction is evaluated for typical fibrous types of debris, such as NUKON, with respect to two size classes. The result shows a considerable increase in the debris transport fraction when a turbulence effect is implemented compared to when it is not. Increases of 5.55 and 2.06 times are observed for large NUKON and small/fine NUKON, respectively. This result implies that the turbulence effect should be considered in the debris transport quantification for conservatism. It was also found that the debris transport fraction may change depending on which sump is active between the two sumps. For example, small/fine NUKON is much more transportable when a sump near the break operates compared to when a sump far from the break operates. This fact also implies that the location of the active sump should be considered as an important parameter in comprehensive debris transport evaluations given a maximum head loss at the sump screen.

© 2012 Elsevier B.V. All rights reserved.

1. Introduction

Debris generated by a high-energy pipe line break accident such as a loss-of-coolant accident (LOCA) could endanger the cooling capability of a pressurized water reactor (PWR) during the recirculation phase of long-term cooling by the blocking recirculation sump screen. That is, a clogged sump screen due to debris could reduce the available net positive suction head (NPSH) of safety

* Corresponding author at: School of Mechanical Engineering, Pusan National University, Jangjeon-dong, Geumjeong-gu, Busan 609-735, Republic of Korea.
Tel.: +82 51 510 3050; fax: +82 51 512 5236.
E-mail address: jihwan@pusan.ac.kr (J.H. Jeong).

0029-5493/$ – see front matter © 2012 Elsevier B.V. All rights reserved.
http://dx.doi.org/10.1016/j.nucengdes.2012.05.022

injection pumps. As a result, the operability of the safety system during the recirculation cooling phase is likely to be jeopardized. This safety issue was designated as GSI-191 in the U.S., and many studies to resolve this issue have been undertaken (USNRC, 2003a). The regulatory guide 1.82, revision 3, requires a specific analysis with respect to screen blockage of the water recirculation sump. In particular, all debris transport mechanisms should be analyzed, including the blow-down, wash-down, pool fill-up and the recirculation mode mechanisms when evaluating debris generation and debris transport.

One-dimensional (1D) lumped-parameter codes have usually been utilized in analyses of debris transport after a LOCA (USNRC, 2004). These 1D lumped-parameter codes do not consider the three-dimensional (3D) behavior of discharged coolant or turbulence effects and do not consider the real shape of the containment building. Therefore, the NEI and USNRC recommended using 3D CFD codes for more realistic analysis of LOCA debris transport situations (NEI, 2004; USNRC, 2004). In recent years, the NEI (2004), the USNRC (2004), Maji et al. (2004), Ui and Kasahara (2006), and Bang et al. (2010) all evaluated the fraction of debris transport in the pool fill-up or recirculation transport mode using CFD codes. Park et al. (2011) also evaluated the debris transport fraction for the blow-down phase using a commercial CFD code.

Through previous research on the GSI-191 safety issue, the use of 3D CFD analysis to estimate the debris transport fraction during the recirculation cooling phase has been established as an analytical refinement. In this analytical refinement, the mean fluid velocity distribution within the containment floor is combined with fundamental transport properties of various types of debris to identify the debris transport fraction. To be specific, the debris transport fraction is determined as a ratio of the area exceeding the reference tumbling velocity of specific types of debris to the area of the containment bottom floor. In the determination of the debris transport faction, it is also advised that the turbulent kinetic energy (TKE) distribution of the fluid flow is considered to quantify the debris transport fraction (NEI, 2004; USNRC, 2004), as the effect of the TKE, which augments debris floor transportation by affecting the tumbling velocity of the debris, has been identified in experimental research (Maji et al., 2002, 2004; USNRC, 2002a,b).

Unfortunately, however, the quantification results pertaining to the debris transport fraction during the recirculation cooling phase including debris transport augmentation by TKE were not published in the literature. Therefore, in the present study, the debris transport fraction quantification of the OPR1000 nuclear power plant, which is under operation in Korea, is investigated considering the TKE obtained from a 3-D CFD analysis. Its implication is also discussed.

In the following sections, the CFD analysis result of the OPR1000 nuclear power plant is explained first. Then, experimental verification of the TKE effect is introduced. Next, the quantification of the debris transport fraction with and without TKE implementation is given. Finally, conclusions of the study are given.

2. CFD analysis

2.1. Break and plant modeling

In the GSI-191 safety issue evaluation, the break size and the location of the high-energy pipe were selected on a basis that the maximum head loss across the sump screen would result due to the maximum amount of debris generation and transportation. In accordance with this criterion, a double-ended guillotine break (DEGB) of a hot leg of the OPR1000 plant was selected for a high-energy pipe break in the present study without considering multiple breaks. The present break selection is actually conservative in the following three reasons (KHNP, 1998; NEI, 2004; USNRC, 2004): (i) the zone of influence (ZOI) of a hot leg break (diameter = 42 in.) is larger than the ZOI of a cold leg break (diameter = 36 in.); (ii) it is well known that the steam generator around the hot legs contains the greatest amount of thermal insulation material and that a DEGB generates the largest amount of debris within the ZOI of a hot leg break; (iii) other pipes within the primary cooling system of OPR1000 plant are relatively very small.

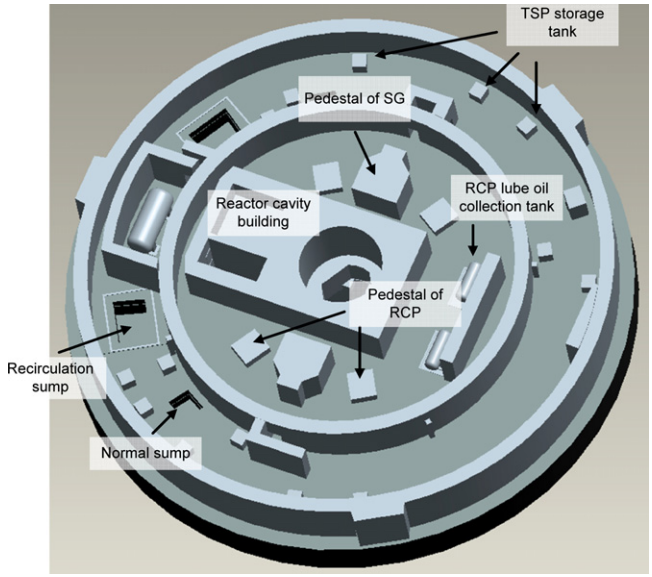

Fig. 1. 3-D CAD model of the OPR1000 containment (EL. 26.21 m).

The containment building of the OPR1000 consists of an inside building of which diameter and thickness are respectively 29.26 m and 1.2 m and an outside building of which diameter is about 43.28 m. Therefore, the bottom floor is composed of a circular inside space and an annular space surrounding the inside space. In the circular inside building, there are various structures, including the reactor cavity, two steam generator supports, four reactor-coolant-pump (RCP) supports and the RCP lube oil collection tanks. In the annulus outside building, two recirculation sumps, two normal sumps and sixteen TSP storage tanks are located. As these structures affect the fluid flow during the recirculation cooling phase, 3D computer-aided drawing (CAD) models of all of the structures were generated using a 3D CAD tool. Fig. 1 shows the 3-D CAD model used in the present CFD analysis. The modeled computational domain ranges from the containment bottom floor, with an elevation of 26.21 m, to the center of hot leg, with an elevation of 32.00 m. In total, 2.5 million structured meshes were used in the analysis as shown in Fig. 2, of which the average size is about 0.08 m. Furthermore, the meshes are clustered densely around the break inflow, the sump intake and the steam generator support regions for accuracy based on a preliminary mesh dependency study.

2.2. Numerical analysis

In previous CFD analyses of the recirculation cooling phase, an artificial slip boundary condition was used for the water surface of the containment floor (NEI, 2004; USNRC, 2004). As a result, the effect of free surface motion was likely suppressed. Therefore, in the present study, all features of the free-surface motions of the containment floor water are simulated by the FLOW-3D commercial CFD code, as this software is equipped with a volume of fluid (VOF) scheme able to give a more realistic analysis of the free

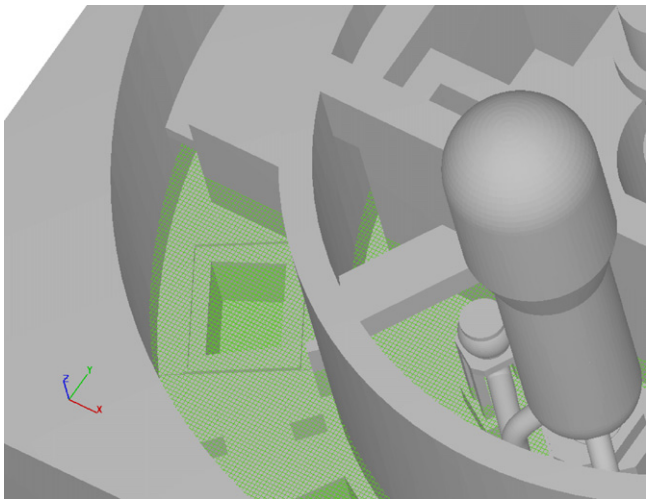

Fig. 2. Meshes around the recirculation sump.

surface flow. The governing equations adopted in FLOW-3D code are given below.

$$V_F \frac{\partial \rho}{\partial t} + \frac{\partial}{\partial x}(\rho u A_x) + \frac{\partial}{\partial y}(\rho v A_y) + \frac{\partial}{\partial z}(\rho w A_z) = 0 \quad (1)$$

$$\frac{\partial u}{\partial t} + \frac{1}{V_F}\left(uA_x\frac{\partial u}{\partial x} + vA_y\frac{\partial u}{\partial y} + wA_z\frac{\partial u}{\partial z}\right) = -\frac{1}{\rho}\frac{\partial p}{\partial x} + G_x + f_x \quad (2a)$$

$$\frac{\partial v}{\partial t} + \frac{1}{V_F}\left(uA_x\frac{\partial v}{\partial x} + vA_y\frac{\partial v}{\partial y} + wA_z\frac{\partial v}{\partial z}\right) = -\frac{1}{\rho}\frac{\partial p}{\partial y} + G_y + f_y \quad (2b)$$

$$\frac{\partial w}{\partial t} + \frac{1}{V_F}\left(uA_x\frac{\partial w}{\partial x} + vA_y\frac{\partial w}{\partial y} + wA_z\frac{\partial w}{\partial z}\right) = -\frac{1}{\rho}\frac{\partial p}{\partial w} + G_z + f_z \quad (2c)$$

Here, V_F is the fractional volume open to the flow, ρ is the fluid density, p is the pressure, and u, v, w are the velocity components in the coordinate directions of x, y, z. A_x is the fractional area open to the flow in the x-direction, and A_y and A_z are similar area fractions for the flows in the y and z directions, respectively. G_x, G_y, G_z denote the body accelerations, and f_x, f_y, f_z are the viscous accelerations. Fluid configurations are defined in terms of the volume of fluid function, F. This function represents the volume of fluid #1 per unit volume and satisfies Eq. (3),

$$\frac{\partial F}{\partial t} + \frac{1}{V_F}\left[\frac{\partial}{\partial x}(FA_x u) + \frac{\partial}{\partial y}(FA_y v) + \frac{\partial}{\partial z}(FA_z w)\right] = 0 \quad (3)$$

where F represents the volume fraction occupied by the fluid. Thus, fluid exists where F is 1, while void regions correspond to the locations where F is 0. For the pressure calculations, the generalized minimum residual method (GMRES) is applied to the continuity and momentum equations. For turbulence modeling, the re-normalized group (RNG) k–ε model is used in the present CFD analysis because this model has shown better results with respect to swirl flows as compared to the standard k–ε model (NEI, 2004; USNRC, 2004).

A transient analysis of the fluid flow for the containment pool that forms during the recirculation cooling phase was performed for 400 s after the recirculation actuation signal (RAS) by adopting the VOF scheme with a time step size of 0.05 s. The hot leg break location was selected as the inlet flow boundary, and the inlet flow was modeled as a free falling stream originating from the center of the hot leg break (elevation of 32.0 m) without any interference from other structures (NEI, 2004). The inlet flow rate was assumed to be 0.40 m^3/s, which was the sum of the high-pressure safety injection (HPSI) flow rate, 0.08 m^3/s, and the containment spray

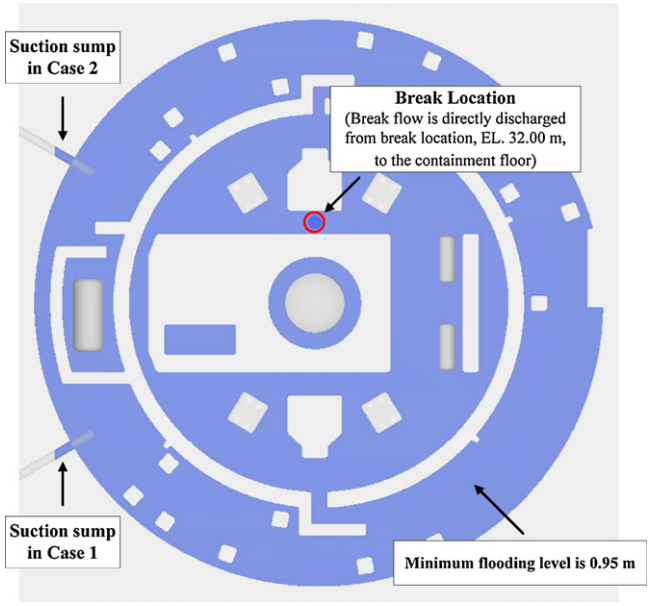

Fig. 3. Boundary and initial conditions for 3-D CFD analysis.

(CS) flow rate of 0.32 m^3/s (KHNP, 1998). It needs to be noted that this assumption might increase uncertainty in the flow field on the bottom floor since containment sprays would be dispersed in various locations of the containment pool. For the outlet flow boundary, only one of the two recirculation sumps in the OPR1000 plant was assumed to be operable on a conservative basis in the safety analysis. A recirculation sump located far from the break location was assumed to be operable in Case 1, and the other recirculation sump was assumed to be operable in Case 2. A Dirichlet boundary condition, a negative velocity corresponding to inlet flow rate, was applied to the outlet flow. The initial flooding level of the containment floor was assumed to be 0.95 m on a conservative basis of debris transport (NEI, 2004; USNRC, 2004) with reference to minimum flooding level (about 1.00 m) in the final safety analysis report (FSAR) of the OPR1000 plant (KHNP, 1998). The rest of the containment was assumed to be filled with air of 115.83 kPa (KHNP, 1998). Fig. 3 shows the boundary and initial conditions in this simulation.

2.3. Characteristics of the mean flow and turbulent kinetic energy

During the recirculation cooling phase of a LOCA, a break flow is introduced to the floor of the inside building first. It then flows rapidly along the side of the reactor cavity building (see location 1 in Fig. 4). Next, a high-velocity flow field begins to form near the active recirculation sump due to the suction of the outlet flow boundary (location 2) and the open area of the annular barrier wall between the inside building and the outside building (location 3). The fluid of the inside building then flows azimuthally along the inside of the circular barrier wall and penetrates into the outside building through the open area (location 4). Finally, the fluid flow to the active sump develops (location 5). These flow characteristics of the mean flow were found to be similar in both Case 1 and Case 2.

According to Regulatory Guide 1.82, revision 3 (USNRC, 2003a), a steady state or quasi-steady state condition should be used to quantify debris transport in the recirculation cooling phase. Because the flow velocity field close to the open area shows numerous changes and a high value, the velocity and TKE of the corresponding region is monitored (see Fig. 5). It was found that a quasi-steady state is approached after about 300 s in the beginning of the simulation.

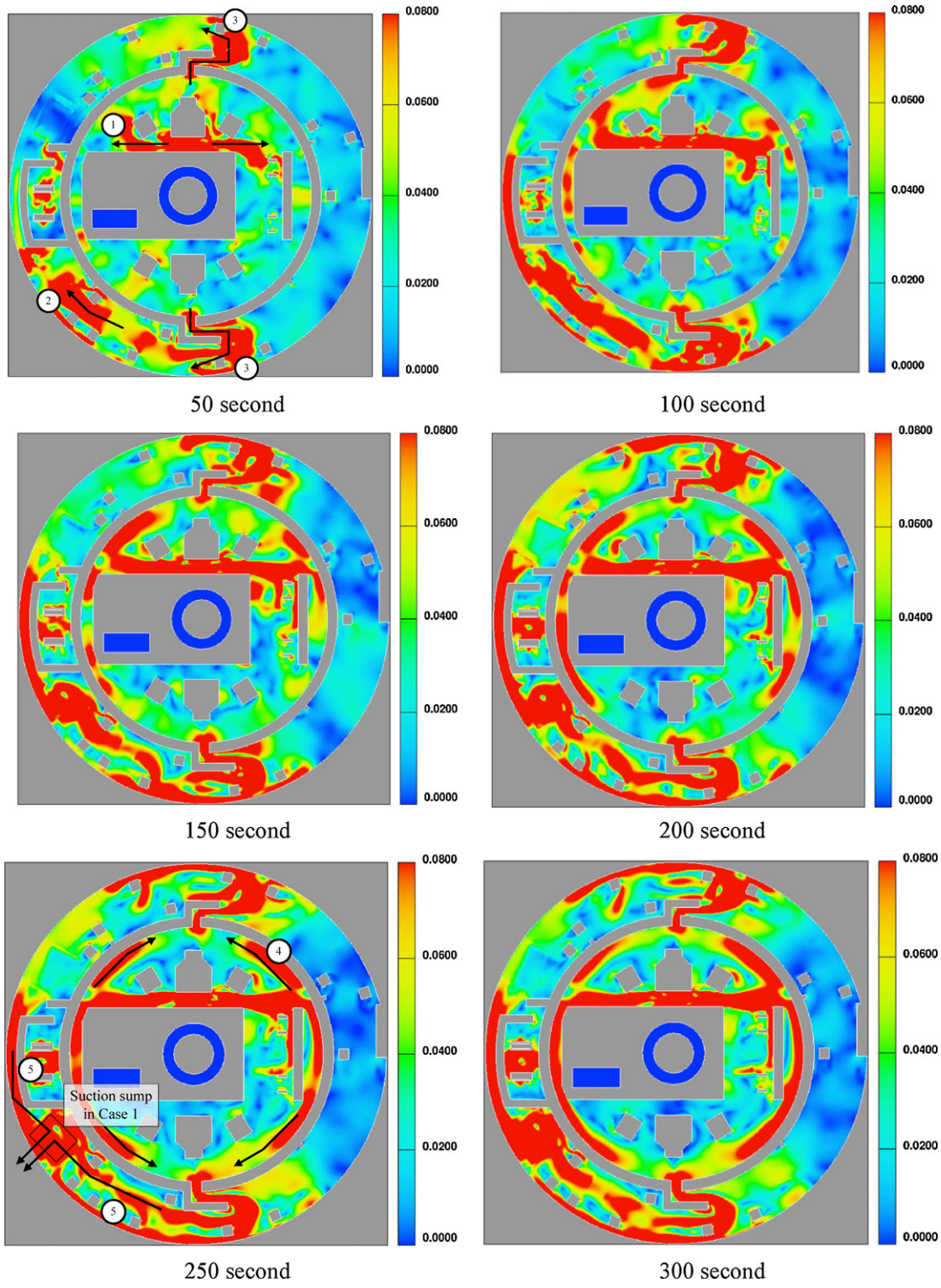

Fig. 4. Flow development within the containment floor during long-term cooling (EL. 27.01 m).

Based on this observation, the CFD result at 400 s is used for the debris transport quantification in the following section.

Regarding the TKE, it was found that the development of the TKE is similar to that of the mean flow during the recirculation cooling phase. A strong TKE is observed at the inlet flow region with high flow fluctuation and the open area region under a high velocity (see Fig. 6). Furthermore, a relatively high TKE is noticed near the structures of the steam generator supports, RCP supports and the TSP storage tank.

3. Experimental verification of the TKE effect

The effect of turbulent kinetic energy on the augmentation of debris floor transport was observed in several experimental

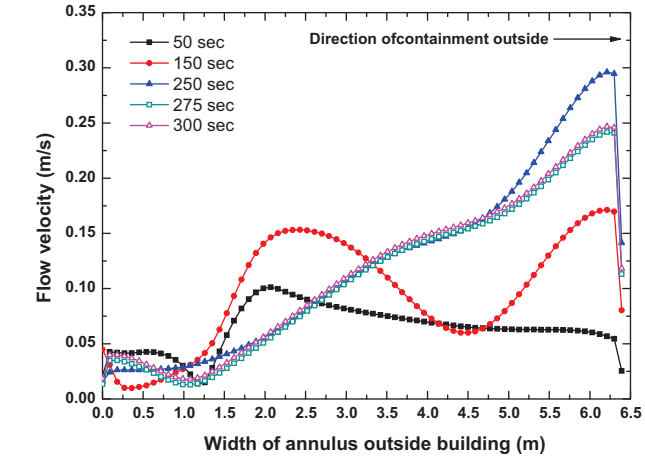

(a) Velocity profiles

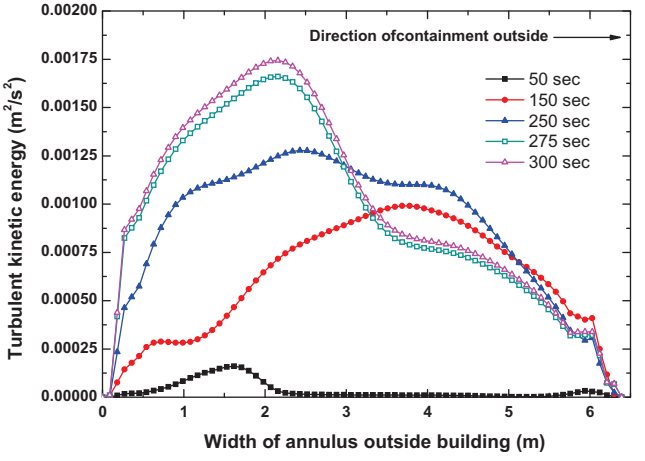

(b) TKE profiles

Fig. 5. Velocity (a) and TKE (b) profiles around the open area of the annular barrier wall (EL. 27.01 m).

studies (Maji et al., 2002, 2004; USNRC, 2002a,b). Its application to the evaluation of the debris transport was highly recommended (NEI, 2004; USNRC, 2004). Unfortunately, however, a specific detailed method of implementing TKE in conjunction with a CFD analysis result to determine debris transport remains unknown except for the NUREG/CR-6369 report (USNRC, 1999), in which the application of TKE for determining debris suspension using $u_{rms} = \sqrt{2 \times TKE}$ was suggested. Therefore, in the following section, through an experiment and supplementary CFD calculations, the TKE effect on the tumbling velocity was identified and its implementation methodology for debris floor transport augmentation was suggested.

3.1. Experimental test facility and methods

To evaluate the TKE effect on debris floor transport, the tumbling velocities should be measured at a quiescent flow condition in which the turbulence is suppressed maximally as a reference and under a turbulent flow condition in which TKE is conspicuous. Therefore, in the present study, a linear flume test facility (Configuration 1) was created with reference to previous research (Maji et al., 2002; USNRC, 2002a) to measure the tumbling velocities in a quiescent flow condition. The facility was also designed to be modified as sudden-expansion and sudden-contraction flume test facilities by installing obstacles made of poly-carbonate to measure the tumbling velocities under turbulent flow conditions (Configuration 2, 3, respectively). A detailed schematic of the test facility is given in Fig. 7. As shown in the schematic, the test facility is a closed-loop type created for considering a conservative flooding height of about 1 m in the OPR1000 plant in the recirculation cooling phase. It is also equipped with mesh screens 0.1 mm in size to dampen the turbulence and a flow diffuser to provide a uniform flow. Water is introduced to the inside of the flume by an inlet pipe which is located at 0.2 m on the free surface and is discharged to an outlet behind the test section. For the circulation of the water, piping of 0.25 m in diameter and a 40 HP centrifugal pump with a 10 m head are used. The flow rate of the facility is regulated by an inverter and measured by a magnetic flow meter which ranges from 10 to 12,000 LPM with ±0.5% accuracy. Furthermore, 0.01 m scale graph paper is attached onto the bottom of the facility to locate the debris specimens and measure their movement.

As the actual debris generated by a LOCA vary in terms of their type, size and shape, it is difficult to conduct direct experiments with them. Therefore, spherical acrylic beads (diameter = 12 mm ± 0.07 mm) and glass beads (diameter = 16 mm ± 0.25 mm) are used as surrogates for the debris in the present experiment (see Fig. 8). The specific weights of the acrylic and glass beads are 1.12 and 2.3, respectively, which are very close to those of K-wool (specific weight 1.4) and NUKON (specific weight 2.5) which are insulation materials in the OPR1000 plant.

The experiment was done while the level of the water in the flume was maintained at 1 m and while locating the bead specimens at predetermined positions on the bottom of the test facility. During the experiments, the flow rate was increased slowly and set constant upon the visual identification of the movement of the beads to determine the exact flow rate. In total, 28 beads (16 for acrylic beads and 12 for glass beads) were used in the experiment. For the Configuration 1 experiment without any turbulence-generating obstacles, the 16 acrylic beads were divided into 4 groups. Each group is composed of 4 acrylic beads randomly sampled from the 16 acrylic beads. Ten repeated tests were performed with each group of acrylic beads in Configuration 1. Similarly, ten repeated tests were also performed for each of the 3 group of glass beads composed of 4 glass beads randomly sampled from the 12 glass beads. For the Configuration 2 experiment with a sudden-expansion obstacle and the Configuration 3 experiment with a sudden-contraction obstacle, randomly sampled acrylic and glass beads were used as test specimens and 10 repeated measurements were performed in each case. Details about the test cases, C, for each experimental Configuration and the locations of the debris specimens, L, for each test case are given in Fig. 9.

3.2. Experiment results

Using the measured flow rate at which debris specimens begin to move and the geometrical section area in which the debris is placed, the minimum and maximum tumbling velocities for every test location of the various experimental configurations are calculated by Eq. (4).

$$\mathrm{TV} = \frac{Q}{H \times W} = \frac{Q}{A_g} \tag{4}$$

Here, TV (TV) is the minimum or maximum tumbling velocity of the debris, Q is the measured mean flow rate, and H, W and A_g are the height of water, the width of the test flume and the geometrical section area in which debris specimens are located, respectively. The TV was determined based on a translational movement through a distance of debris.

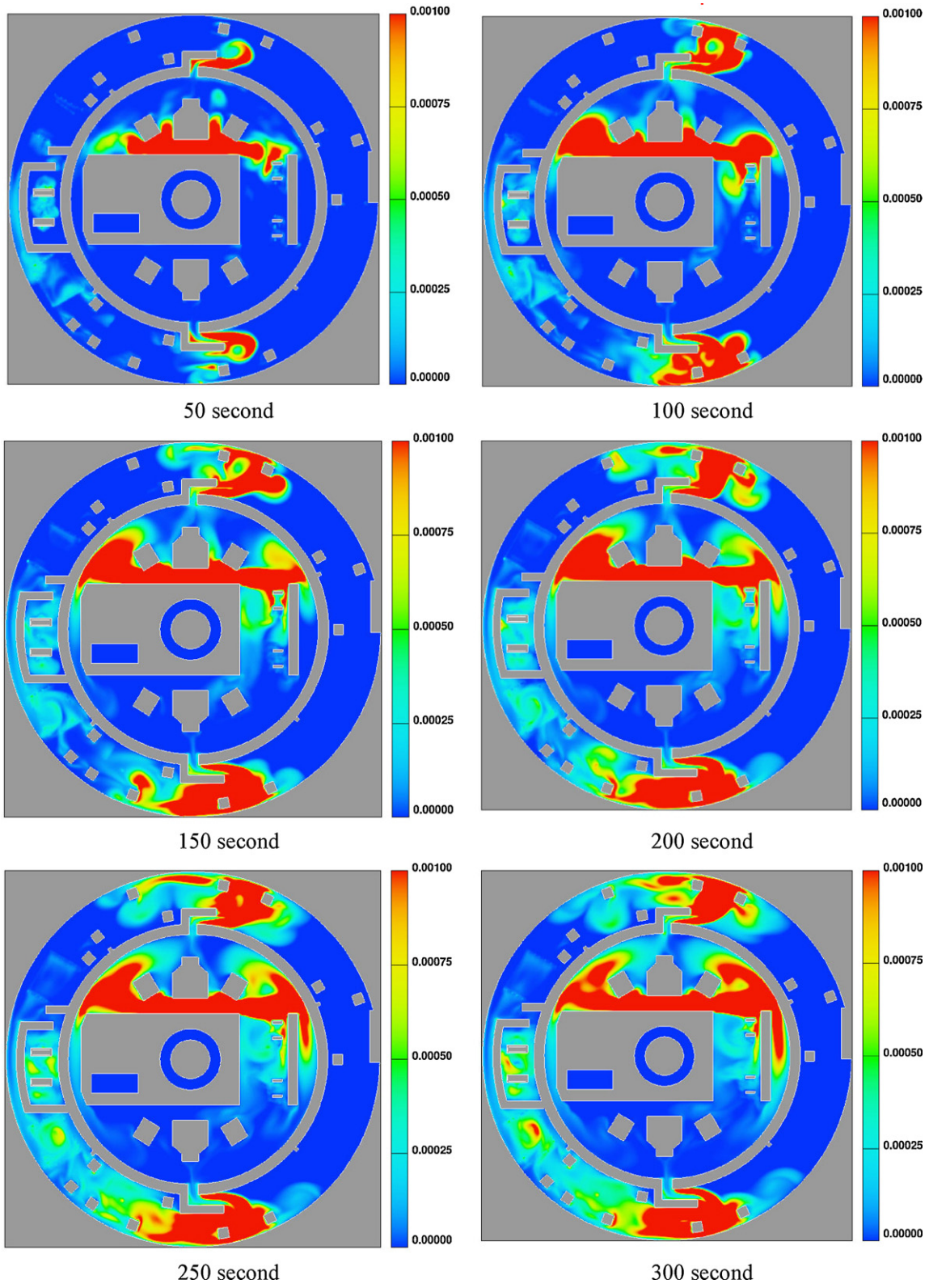

Fig. 6. TKE development of within the containment floor during long-term cooling (EL. 27.01 m).

Table 1 shows the minimum and maximum TVs calculated by Eq. (4). For the experimental Configuration 1, C-1, the TV for the acrylic beads was determined to range from 0.042 m/s to 0.056 m/s; it ranges from 0.116 m/s to 0.134 m/s for the glass beads. The table shows that the TVs of the various test locations for experimental Configurations 2 and 3, C-2 and C-3, are similar to those of Configuration 1, except for a few test cases. The test case C-2-2 and C-2-3 of the experimental Configuration 2 and test case

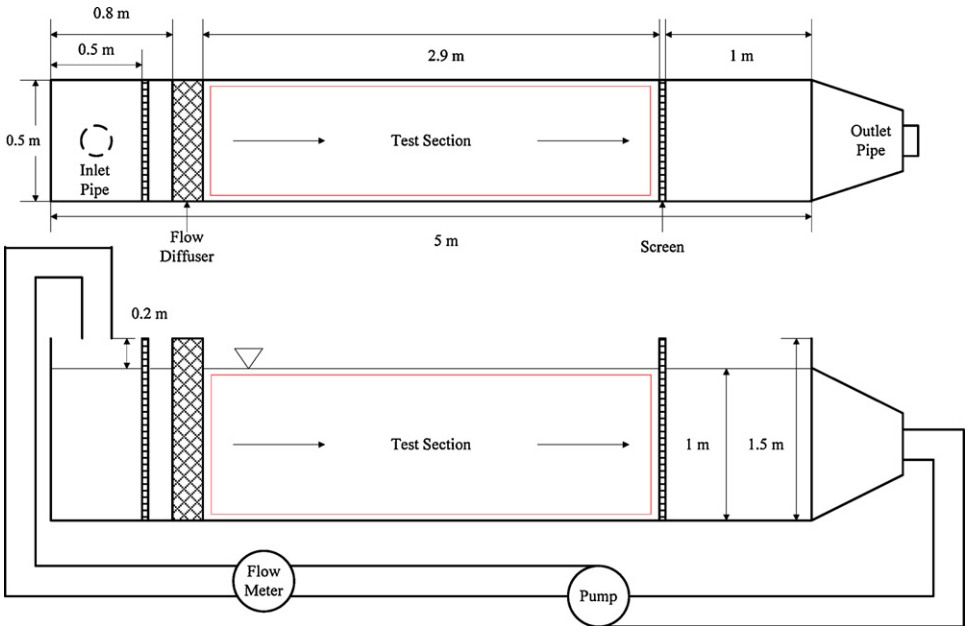

Fig. 7. Schematic of the linear flume test facility.

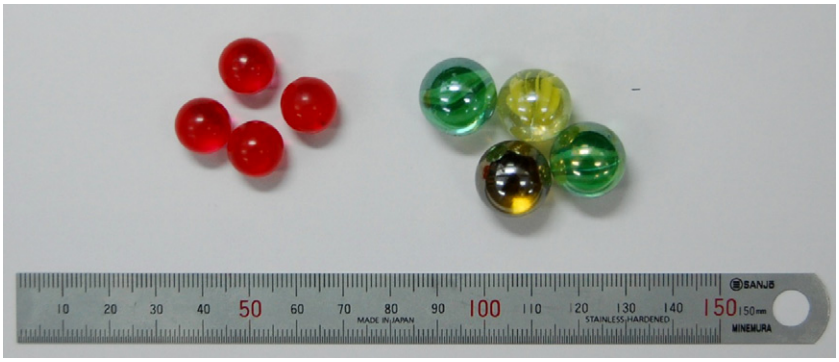

Fig. 8. Debris surrogates (acrylic and glass beads).

C-3-2 and C-3-3 of the experimental Configuration 3 show relatively low TVs. There are two possible reasons for this discrepancy. One is that the geometrical section area used in Eq. (4) cannot reflect the area reduction effect due to flow recirculation after the obstacle in Configuration 2 and flow detachment before the obstacle in Configuration 3. The other reason could be a turbulence effect, as the vigorous turbulence is likely to be enhanced by obstacles in the experimental Configurations 2 and 3 (Yakhot et al., 2006). To confirm these conjectures, supplementary CFD analyses are performed. Meanwhile, the debris location L4 of C-2-2 and C-2-3 of the experimental Configuration 2 show relatively high TVs. The reasons will be discussed in Section 3.3.

3.3. Supplementary CFD analysis and identification of the TKE effect

Supplementary CFD analyses were performed for the experimental Configurations 1, 2 and 3. Fig. 10 shows the 3D CFD model used as the simulating experimental facility. The real geometry with flow diffuser was used and the mesh screen was represented with a one-dimensional porous media in this study. The inlet flow was modeled as a free falling from the exit of inlet pipe, located 0.20 m high from water level as the same as the experimental condition. The initial water level of the flume was modeled to be 1.00 m. Around 500,000 structured meshes of a size of 0.01 m × 0.01 m × 0.03 m were used. Flow velocity was specified at the inlet and outlet. The CFD simulations were performed with water flow rates corresponding to minimum TVs as well as maximum TVs for each debris location for all experimental cases. The CFD analyses were performed using the FLOW-3D code with the VOF scheme. The time step size employed was 0.5 s and a transient analysis was done up to 200 s because a quasi-steady state was established after 150 s. Because supplementary CFD analyses were conducted under the same boundary and initial conditions as the experiments, the calculated results were used as reasonable surrogates of the physical experiment in the present study.

Fig. 11 shows the flow velocities for Configuration 1 based on supplementary CFD results. The flow velocity seems to be nearly uniform due to mesh screen and flow diffuser. Fig. 12 shows the streamlines of the flow for Configurations 2 and 3, respectively.

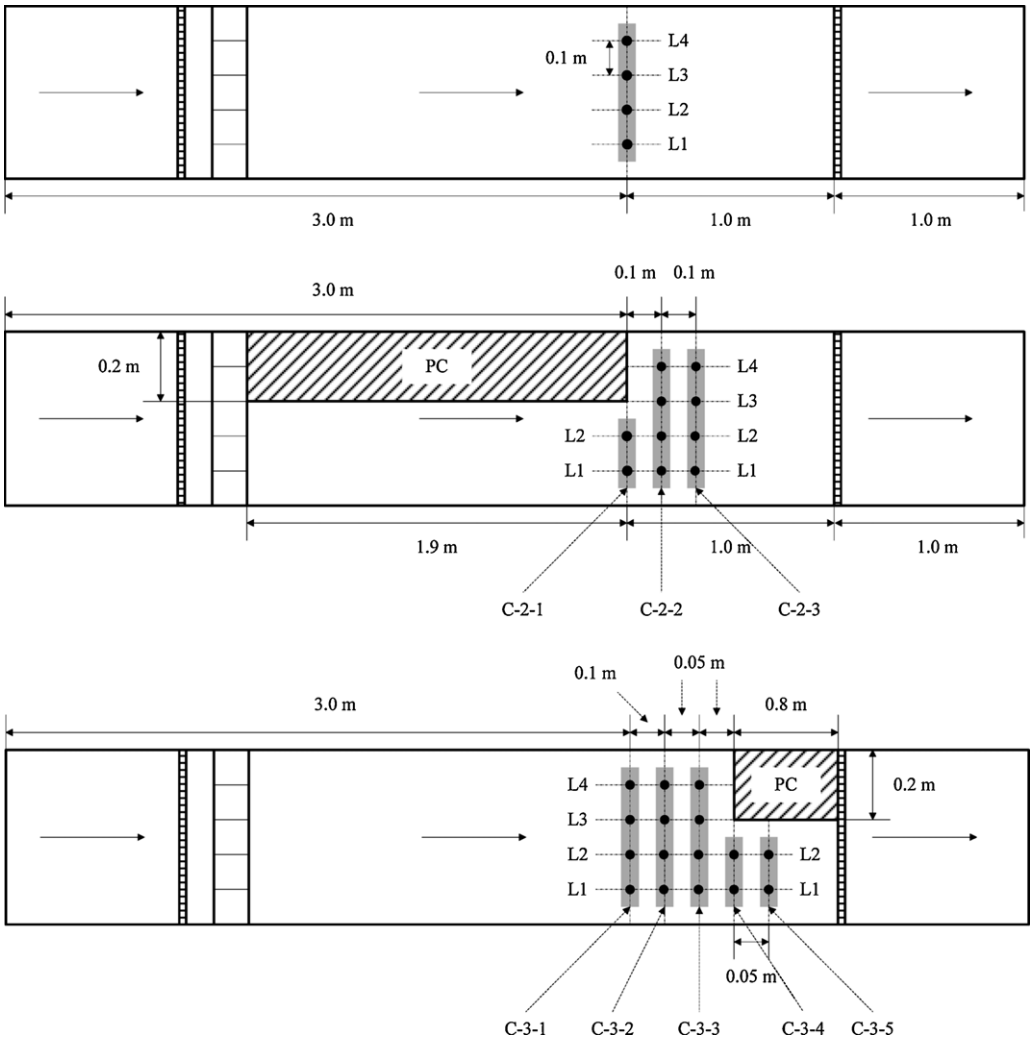

Fig. 9. Locations of the debris specimens and identifications in experimental Configurations 1, 2 and 3.

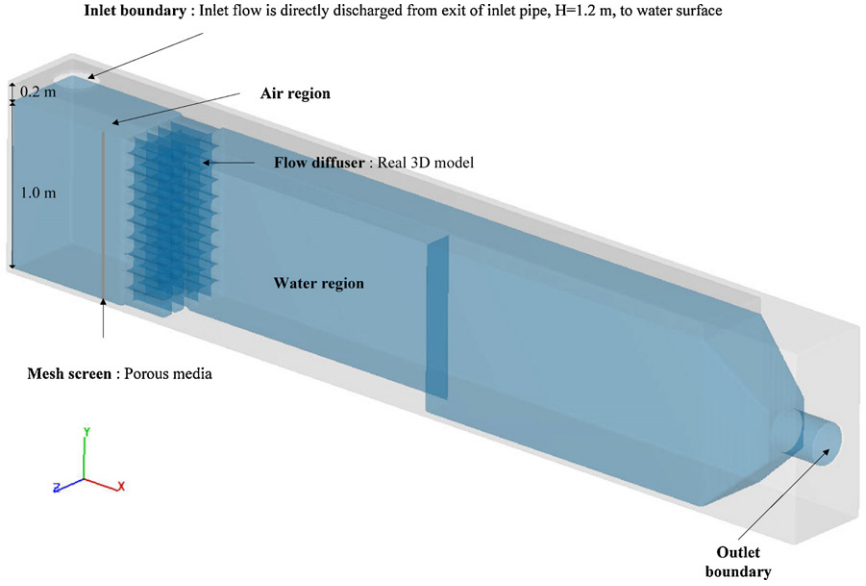

Fig. 10. 3-D CFD model (sudden-expansion flume).

Table 1
Tumbling velocities of acrylic and grass beads.

Test cases		Debris locations	Acrylic beads		Grass beads	
			Min. TV (m/s)	Max. TV (m/s)	Min. TV (m/s)	Max. TV (m/s)
Configuration 1 (reference)	C-1	L1	0.042	0.056	0.121	0.128
		L2	0.043	0.055	0.116	0.134
		L3	0.042	0.056	0.121	0.128
		L4	0.044	0.056	0.121	0.134
Configuration 2	C-2-1	L1	0.040	0.053	0.114	0.127
		L2	0.041	0.053	0.112	0.127
	C-2-2	L1	0.021	0.028	0.061	0.069
		L2	0.023	0.027	0.059	0.069
		L3	0.024	0.027	0.062	0.067
		L4	0.112	0.128	0.326	0.354
	C-2-3	L1	0.023	0.027	0.063	0.068
		L2	0.023	0.028	0.061	0.066
		L3	0.023	0.027	0.062	0.067
		L4	0.111	0.130	0.324	0.351
Configuration 3	C-3-1	L1	0.040	0.051	0.117	0.126
		L2	0.041	0.052	0.116	0.128
		L3	0.041	0.055	0.117	0.125
		L4	0.040	0.054	0.116	0.126
	C-3-2	L1	0.037	0.043	0.100	0.103
		L2	0.038	0.042	0.096	0.104
		L3	0.036	0.041	0.097	0.102
		L4	0.036	0.041	0.097	0.102
	C-3-3	L1	0.023	0.031	0.069	0.076
		L2	0.023	0.031	0.070	0.077
		L3	0.027	0.031	0.071	0.074
		L4	0.032	0.037	0.102	0.105
	C-3-4	L1	0.042	0.046	0.120	0.124
		L2	0.041	0.049	0.120	0.123
	C-3-5	L1	0.042	0.051	0.121	0.122
		L2	0.041	0.048	0.122	0.124

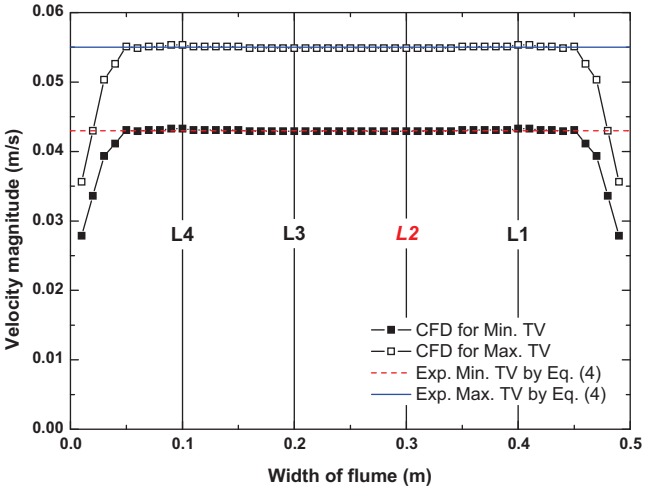

Fig. 11. Flow velocity for Configuration 1 (acrylic beads).

They show that the effective section areas at C-2-2, C-2-3, C-3-2 and C-3-3 are greatly reduced by the flow recirculation in Configuration 2 and by flow detachment in Configuration 3. Table 2 shows the quantitative effective section areas recalculated from the supplementary CFD analyses. The effective section area decreases to approximately 60% of the original geometrical section area at C-2-2, C-2-3 and C-3-3, and it decreases to approximately 80% at C-3-2. Fig. 13 shows velocity magnitude profiles of Configuration 2. Velocity magnitude profiles in Fig. 13(a), (b), (c) were obtained with water flow rates corresponding to TVs at location L2 for cases of C-2-1, C-2-2, and C-2-3, respectively. Fig. 13(d) was constructed in the same way but with water flow rate corresponding to TV at

Table 2
Comparison of the geometric flow area and effective flow area.

Test cases	Geometrical flow area (m^2)	Effective flow area (m^2)
C-2-1	0.3	0.3
C-2-2	0.5	0.3
C-2-3	0.5	0.3
C-3-1	0.5	0.5
C-3-2	0.5	0.4
C-3-3	0.5	0.3
C-3-4	0.3	0.3
C-3-5	0.3	0.3

location L4, which is inside a flow recirculation region. Similar plots was made for Configuration 3 and shown in Fig. 14. These plots show that the flow velocity in a recirculation region is relatively low while the velocity of bulk region is higher than TVs calculated by Eq. (4). It is caused by Eq. (4) which considers geometrical section area rather than local velocity. These figures also show that velocity profile is not uniform across bulk flow region. These observations suggest that tumbling velocity need to be evaluated based on a local average velocity instead of the average velocity based on total cross-sectional area. Using local average flow velocity, the TVs were recalculated using Eq. (5) and presented in Figs. 15 and 16.

$$TV' = \overline{V_{local}} \quad (5)$$

Here, $\overline{V_{local}}$ represents a local area averaged velocity, which is evaluated based on CFD analysis results for the cross-section above a test bead.

As shown in Figs. 15 and 16, the newly defined tumbling velocity, TV′, at bulk flow region for Configurations 2 and 3 (locations L1 and L2) become closer to the reference values (noted as R in abscissa),

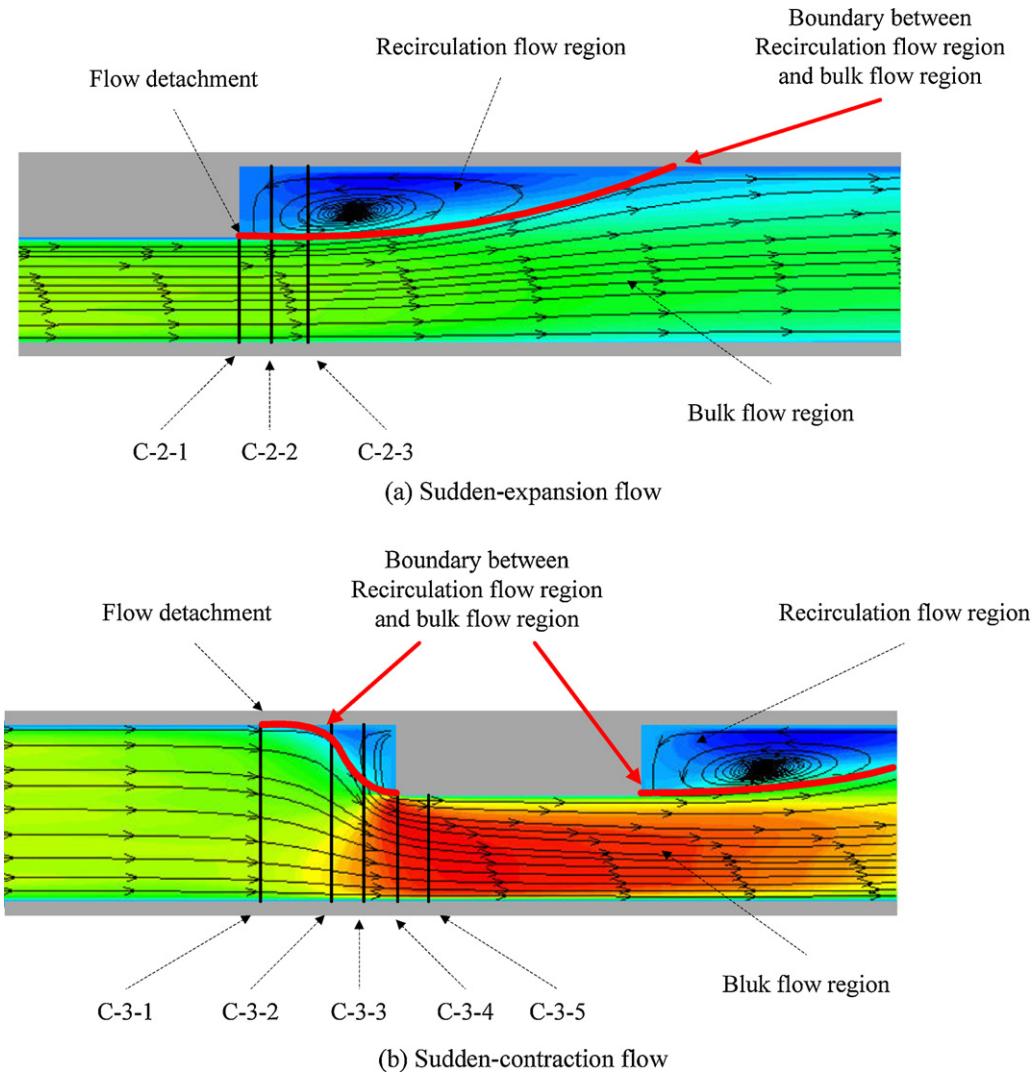

Fig. 12. Streamline of sudden-expansion (a) and sudden-contraction (b) flow.

i.e., those of the Configuration 1. Even though the TV′s at recirculation flow region and its boundary (locations L3 and L4) also become closer to the reference TV, the discrepancy between TV′ and the reference TV is relatively larger than others. These plots also show that tumbling velocities based on Eq. (5) are larger than tumbling velocities based on Eq. (4) except for C-2-2-L4 and C-2-3-L4 to become closer to the reference TV while tumbling velocities for C-2-2-L4 and C-2-3-L4 based on Eq. (5) appeared to be significantly reduced than tumbling velocities based on Eq. (4). However, in spite of this improvement, the tumbling velocities remain slightly lower than the reference values. As indicated before, this may be due to the turbulence effect on the augmentation of debris transport.

Figs. 17–19 show the TKE for Configuration 1, 2, and 3, respectively. The TKE profiles in Figs. 17–19 except for Fig. 18(d) were obtained with water flow rates corresponding to TVs at location L2 for each test case. Fig. 18(d) was constructed in the same way but with water flow rate corresponding to TV at L4. For Configuration 1, the TKE was relatively small and it was nearly suppressed by mesh screen and flow diffuser. For Configuration 2 and 3, the TKE was relatively high within the recirculation flow region and it has maximum value around the boundary between recirculation flow region and bulk flow region. Especially, the TKE at C-2-2-L4 in Fig. 18(d) are very high although the velocity magnitude at these locations are very low (see Fig. 13(d)). The profile of TKE at C-2-3-L4 is similar to TKE at C-2-2-L4.

To verify the turbulence effect, a fluctuating velocity component parallel to the mean flow direction is determined from the TKE (see Figs. 17–19), as shown below, and the algebraic sum of the mean flow velocity and the fluctuating velocity parallel to it is introduced as the effective TV in the present study (Park and Kim, 2009). As the TKE can be represented with an isotropic turbulence assumption ($u^2 = v^2 = w^2$), as shown below,

$$\mathrm{TKE} \equiv \frac{1}{2}(u^2 + v^2 + w^2) \cong \frac{3}{2}u^2 \tag{6}$$

where u, v and w are the fluctuating velocities in x, y and z-directions, respectively, the fluctuating velocity component parallel to the mean flow direction (say, x-direction) is given by

$$u_{rms} \equiv (u^2)^{1/2} = \sqrt{\frac{2}{3}\mathrm{TKE}} \tag{7}$$

Applying the above definition of the effective tumbling velocity to the present study gives the following equation:

$$\mathrm{TV}_{\mathrm{effect}} = \mathrm{TV}' + v_{rms} = \mathrm{TV}' + u_{rms} = \mathrm{TV}' + \sqrt{\frac{2}{3}\mathrm{TKE}} \tag{8}$$

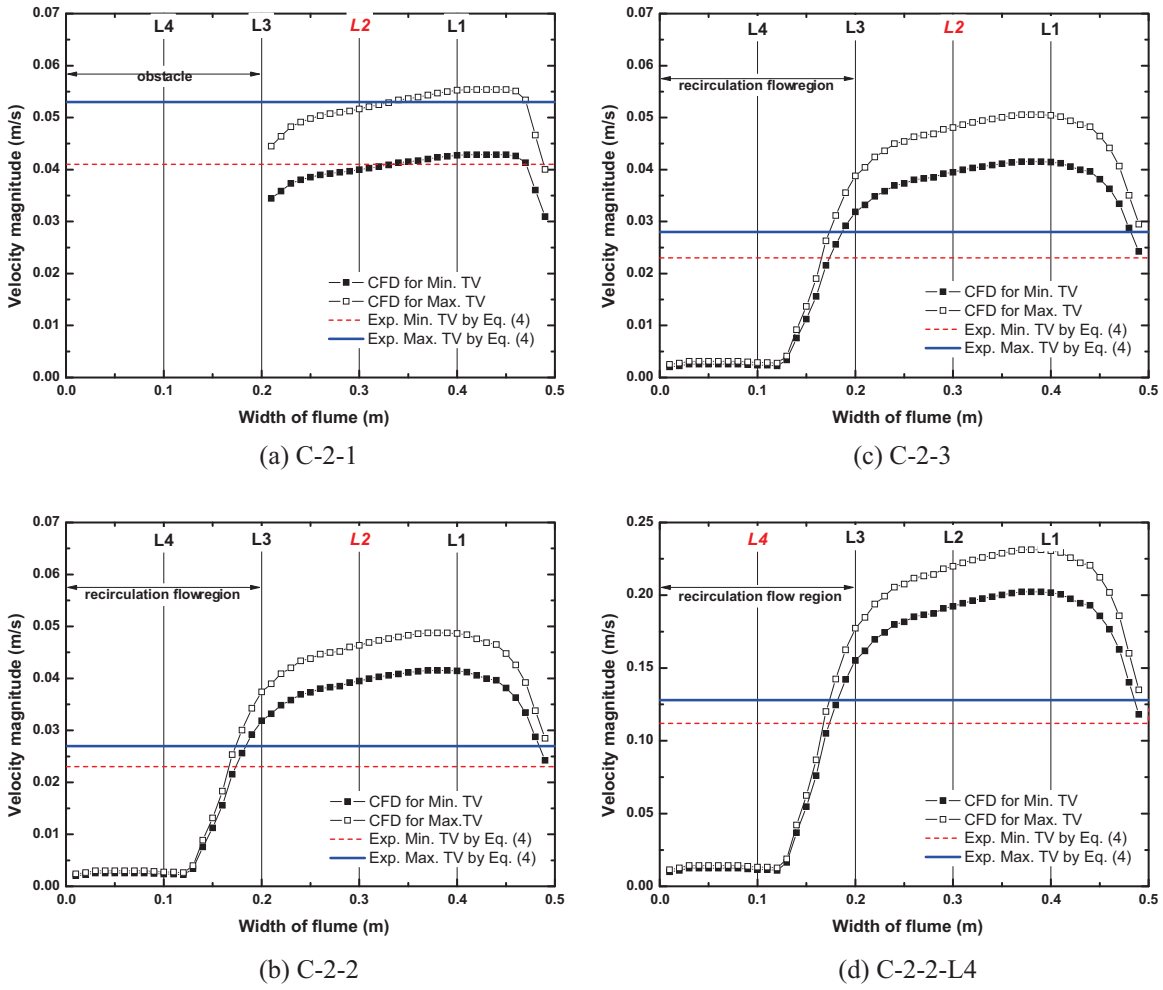

Fig. 13. Flow velocity for Configuration 2 (acrylic beads). (a) C-2-1, (b) C-2-2, (c) C-2-3 and (d) C-2-2-L4.

Table 3
Mean value of effective TVs for the test locations.

Test cases	Mean value of effective TV (m/s)	
	Acrylic beads	Glass beads
C-1 (R)	0.050	0.127
C-2-1	0.050	0.130
C-2-2	0.049	0.127
C-2-3	0.051	0.128
C-3-1	0.049	0.125
C-3-2	0.051	0.126
C-3-3	0.048	0.127
C-3-4	0.049	0.129
C-3-5	0.048	0.130

Here, TV_{effect} is the effective tumbling velocity and v_{rms} is the stream-wise fluctuating velocity. The evaluation result of the above equation using the CFD-calculated TKE is shown in Fig. 20. This plot shows that the effective tumbling velocities of all test locations for various configurations are nearly identical. The mean values of the effective TVs are given in Table 3. The table also shows that the mean values of the effective tumbling velocities of all tests are nearly identical. This fact corroborates that debris transport is augmented by the fluctuating velocity component superimposed on the mean flow direction and is governed by the effective tumbling velocity. The CFD analysis results showed that the contribution of the last term of Eq. (8) to the effective tumbling velocity varied from around 20% to 80% in the recirculation region and its boundary. Based on this finding, the quantification of debris transport due to turbulence is considered in the following section.

4. Quantification of debris transport

As the debris generated by a LOCA varies in the type and size, these factors should be considered together in a quantification of debris transport in the recirculation cooling phase. However, in the present study, only the transport of fibrous types of debris such as NUKON is investigated, as the purpose of the present study is to quantify the debris transport fraction with and without a turbulence effect and because NUKON is known to be mainly a fibrous type of insulation material used in the OPR1000 plant. Because the debris transport characteristics can differ depending on the size of the debris, the size of NUKON is categorized here the two classes of small/fine and large. The transport fractions are also determined for each size class. The reference tumbling velocities measured at a quiescent flow condition for NUKON transport (Maji et al., 2002; USNRC, 2002a, 2003b) are assigned as 0.037 m/s for the small/fine class (0.15 cm pieces) and 0.091 m/s for the large class (0.23 cm pieces).

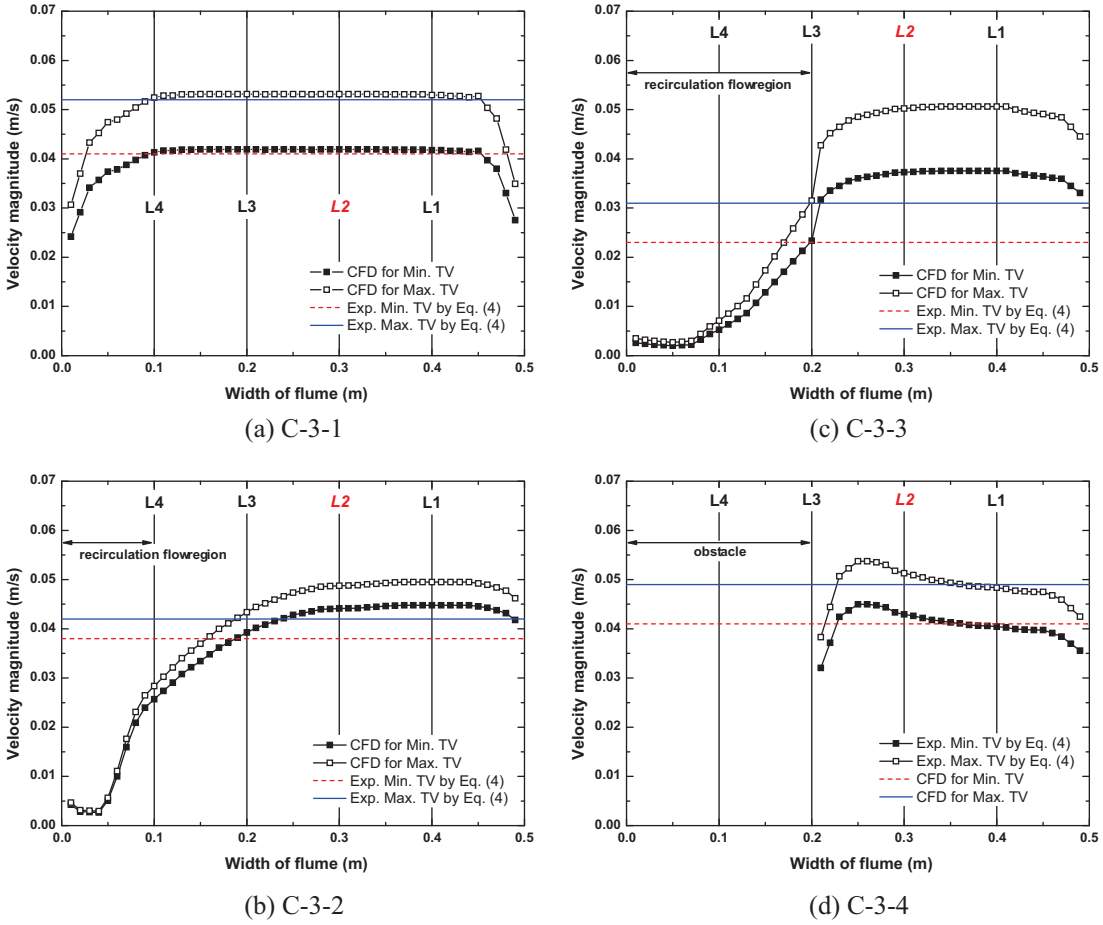

Fig. 14. Flow velocity for Configuration 3 (acrylic beads). (a) C-3-1, (b) C-3-2, (c) C-3-3 and (d) C-3-4.

Table 4
Fraction of debris transport for large NUKON (Case 1).

EL. (m)	Total flooding area (m^2)	Mean flow velocity		Maximum flow velocity	
		Excess area (m^2)	Fraction of debris transport (%)	Excess area (m^2)	Fraction of debris transport (%)
26.41	1079	35.07	3.25	175.55	16.27
26.61		40.79	3.78	183.21	16.98
26.81		42.30	3.92	186.88	17.32
27.01		43.59	4.04	194.11	17.99

Table 5
Fraction of debris transport for small/fine size NUKON (Case 1).

EL. (m)	Total flooding area (m^2)	Mean flow velocity		Maximum flow velocity	
		Excess area (m^2)	Fraction of debris transport (%)	Excess area (m^2)	Fraction of debris transport
26.41	1079	461.60	42.78	499.04	46.25
26.61		466.34	43.22	518.68	48.07
26.81		474.65	43.99	525.15	48.67
27.01		482.10	44.68	529.57	49.08

4.1. Case 1

This case implies that a sump far from the break location operates. The CFD analysis results are described in Fig. 4. The CFD analyses were revisited to evaluate the horizontal mean velocity, V_{mean}, and the maximum horizontal mean velocity, V_{max}. The V_{mean} value represents the mean velocity without consideration of the turbulence effect, and V_{max} represents the maximum mean with consideration of the turbulence effect. V_{mean} is defined as

$$V_{mean} \equiv \sqrt{U^2 + V^2} \quad (9)$$

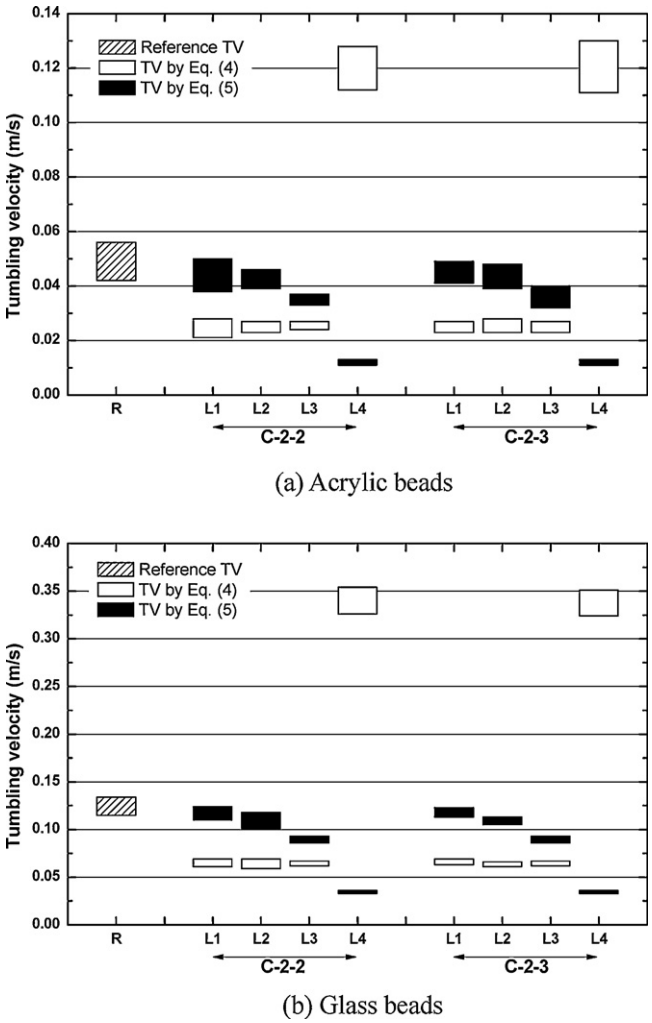

Fig. 15. TVs based on the local area averaged flow velocity for a sudden-expansion flume. (a) Acrylic beads and (b) glass beads.

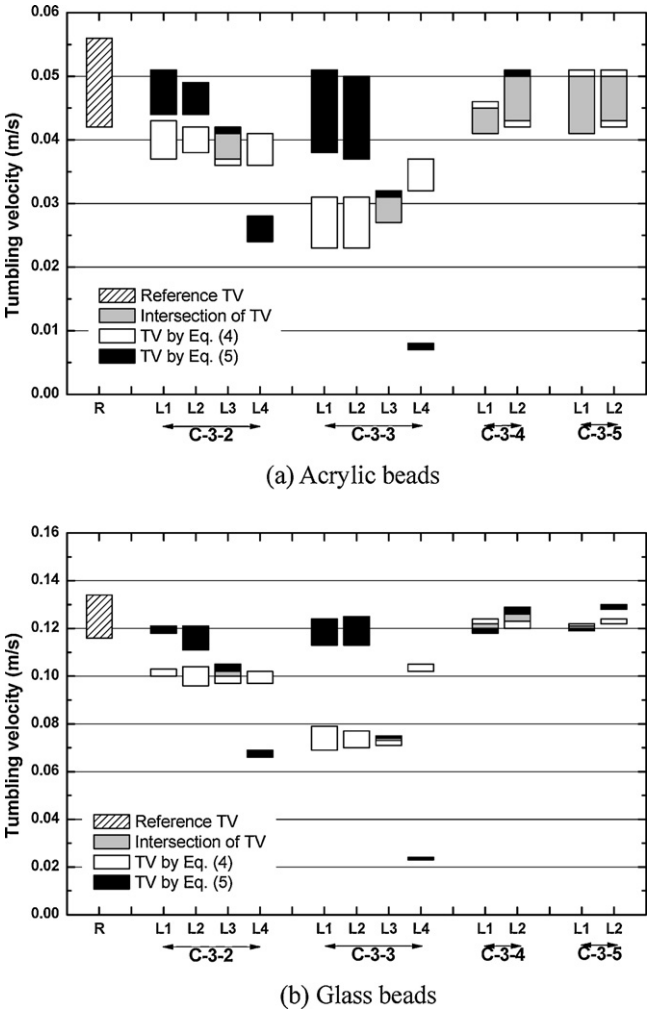

Fig. 16. TVs based on the local area averaged flow velocity for a sudden-contraction flume. (a) Acrylic beads and (b) glass beads.

where U and V denote the horizontal velocity components in the x and y coordinate directions, respectively. V_{max}, which corresponds to the effective TV in Section 3.3, is defined as follows:

$$V_{max} \equiv \sqrt{(U+u_{rms})^2+(V+v_{rms})^2} \equiv \sqrt{\left(U+\sqrt{\frac{2}{3}\mathrm{TKE}}\right)^2+\left(V+\sqrt{\frac{2}{3}\mathrm{TKE}}\right)^2} \quad (10)$$

Figs. 21 and 22 show the change in the area exceeding the reference tumbling velocity depending on the consideration of the turbulence effect. The dark (red) area in Fig. 21(a) represents the area exceeding the reference tumbling velocity (0.091 m/s) for the large NUKON when evaluated based on V_{mean}. This shows that only a part of the exceeded area is linked to the sump suction region continuously and that most of the exceeded area is discontinuous and separated from the sump suction region. This discontinuous area is omitted in the calculation of the debris transport fraction because it implies that the debris is simply stagnant at this region. The area of which V_{max} is larger than the reference tumbling velocity is represented by the dark (blue) area in Fig. 21(b). It shows that the exceeded area is enlarged and that the discontinuity to the sump suction region is diminished. This is due to the fact that V_{max} is inevitably larger than V_{mean} due to the additional turbulence

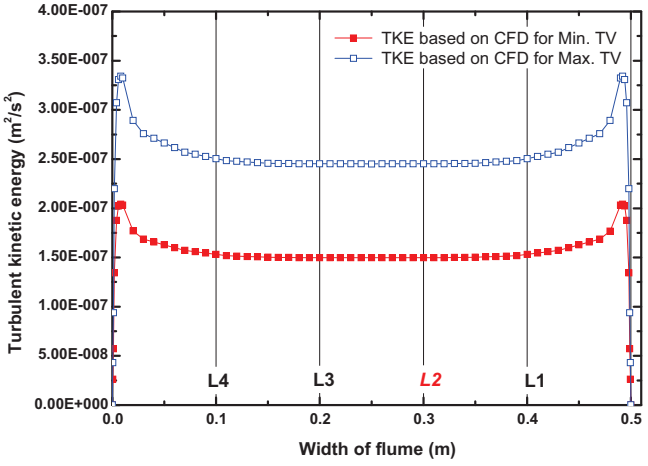

Fig. 17. TKE for Configuration 1 (acrylic beads).

velocity component. Regarding the small/fine NUKON (see Fig. 22), the area exceeding the reference tumbling velocity (0.037 m/s) is also increased when V_{max} is used instead of V_{mean}, but a significant area change or improvement in the discontinuity was not discernible with the large NUKON.

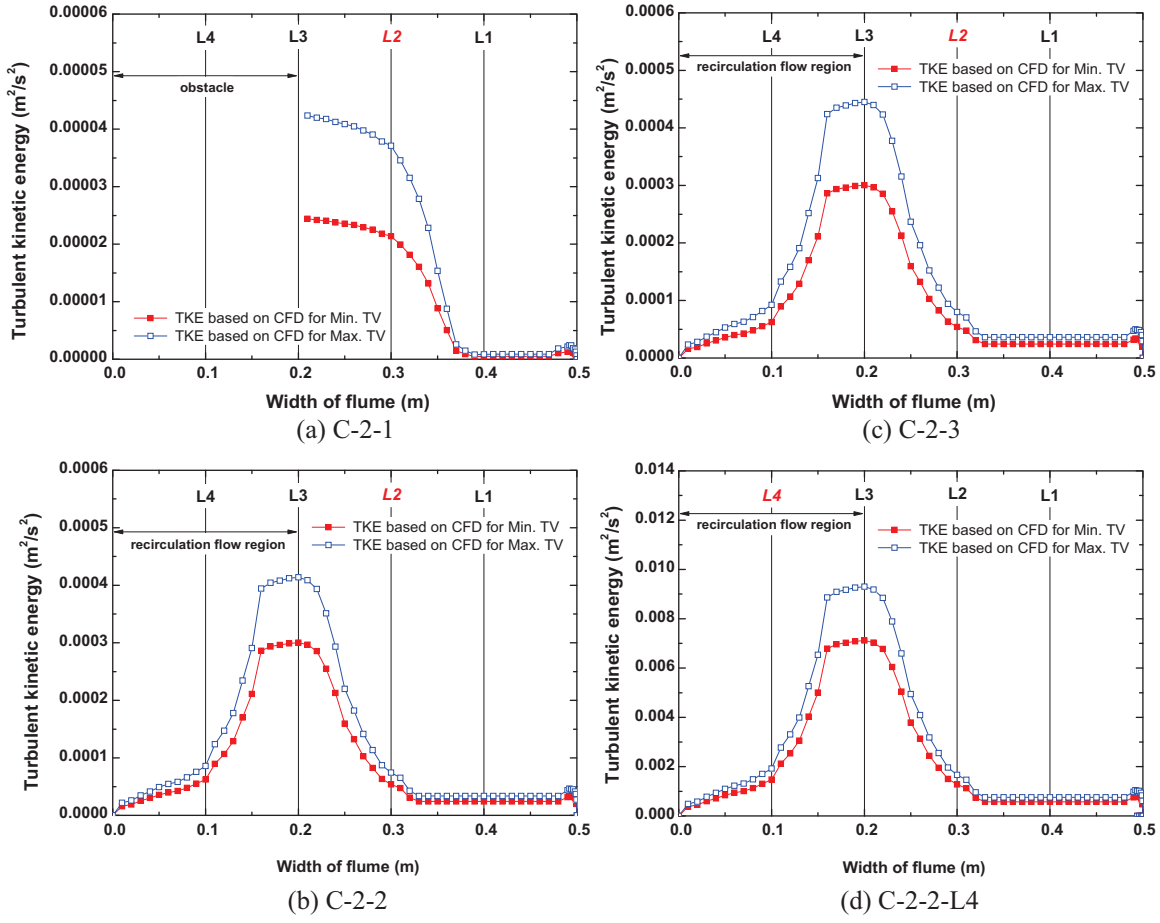

Fig. 18. TKE for Configuration 2 (acrylic beads). (a) C-2-1, (b) C-2-2, (c) C-2-3 and (d) C-2-2-L4.

Table 6
Fraction of debris transport for large NUKON (Case 2).

EL. (m)	Total flooding area (m²)	Mean flow velocity		Maximum flow velocity	
		Excess area (m²)	Fraction of debris transport (%)	Excess area (m²)	Fraction of debris transport
26.41	1079	19.64	1.82	122.36	11.34
26.61		21.36	1.98	125.70	11.65
26.81		24.28	2.25	136.39	12.64
27.01		25.25	2.34	140.16	12.99

Table 7
Fraction of debris transport for small/fine NUKON (Case 2).

EL. (m)	Total flooding area (m²)	Mean flow velocity		Maximum flow velocity	
		Excess area (m²)	Fraction of debris transport (%)	Excess area (m²)	Fraction of debris transport
26.41	1079	264.14	24.48	566.26	52.48
26.61		272.77	25.28	582.23	53.96
26.81		280.22	25.97	588.70	54.56
27.01		287.55	26.65	593.67	55.02

The quantitative NUKON debris transport fractions based on V_{mean} or V_{max} are shown in Tables 4 and 5 for the large and small/fine NUKON, respectively. Here, the transport fraction is evaluated by

$$F(\%) = \frac{A_e - A_d}{A_t} \times 100 \quad (11)$$

where A_e is the excess flow area exceeding the reference tumbling velocity, A_d is the discontinuous area which is not linked to the sump region, and A_t is the total containment recirculation flow area. The transport fraction is calculated at various levels, specifically 0.2 m, 0.4 m, 0.6 m and 0.8 m apart from the bottom of the containment (EL. 26.21 m). It shows an increasing trend as the level becomes higher. Conservatively, the maximum transport fraction

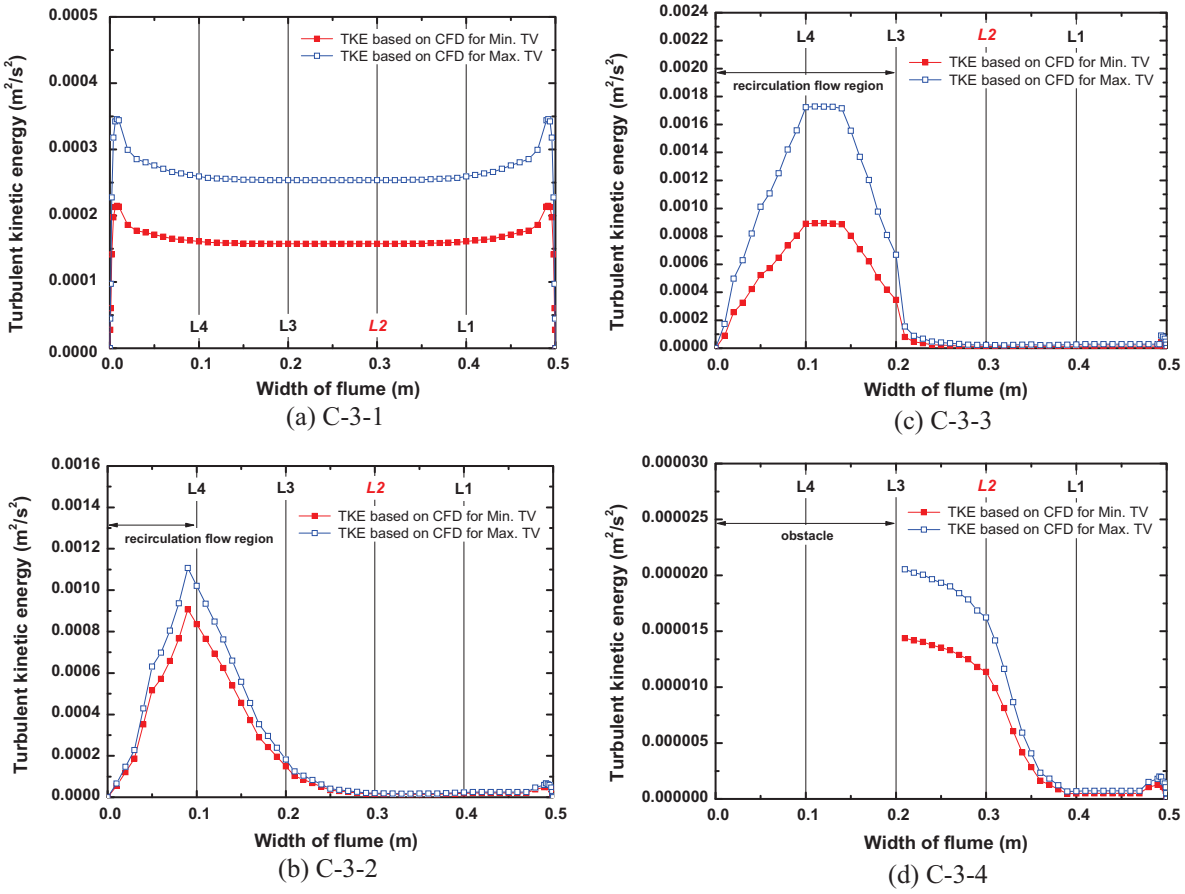

Fig. 19. TKE for Configuration 3 (acrylic beads). (a) C-3-1, (b) C-3-2, (c) C-3-3 and (d) C-3-4.

of the large size is evaluated as 4.04% when determined based on V_{mean}, but it increases to 17.99% if V_{max} is used in the quantification. Regarding small/fine size, transport fractions of 44.68% and 49.08% are obtained based on V_{mean} and V_{max}, respectively. The large increase in the transport fraction of the large NUKON is attributed to the fact that the discontinuous area diminishes sharply if the transport fraction is evaluated based on V_{max}. As there is no abrupt change in the discontinuous area irrespective of the use of V_{mean} or V_{max}, there exists only a minor increase in the transport fraction for the small/fine NUKON.

4.2. Case 2

This is the case at which a sump near the break location operates. Figs. 23 and 24 show the area exceeding the reference tumbling velocity for the large and small/fine NUKON, respectively. For the large NUKON (see Fig. 23(a)), only a small part of the area exceeding the reference tumbling velocity (0.091 m/s) is continuous to the suction sump when evaluated based on V_{mean}. However, the continuous excess area appears to increase sharply when V_{mean} is used (Fig. 23(b)) as the basis of a debris transport evaluation. This occurs mainly because the excess area located in the upper annular area becomes connected to the suction sump. Regarding the small/fine NUKON (see Fig. 24), only the upper part of the excess area appears to be continuous to the suction sump when V_{mean} is used, but almost all of the excess area becomes continuous when V_{max} is used. As a result, the corresponding transport fraction increases sharply.

The quantitative NUKON debris transport fractions based on V_{mean} or V_{max} are shown in Tables 6 and 7 for Case 2. Table 6

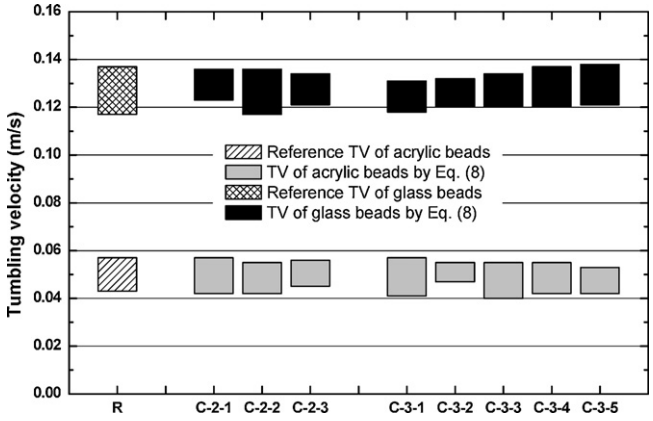

Fig. 20. Effective TVs for the test locations.

shows that the maximum transport fraction of the large NUKON is 2.34% based on V_{mean} but increases to 12.99% when evaluated based on V_{max} for the quantification. Table 7 shows that the transport fraction of the small/fine NUKON increases from 26.65% to 55.02% when evaluated based on V_{mean} and V_{max}, respectively. The large increase in the transport fraction for the small/fine NUKON in Case 2 compared to Case 1 is attributed to the fact that most of the discontinuous area located at the lower part becomes connected when the transport fraction is evaluated based on V_{max}.

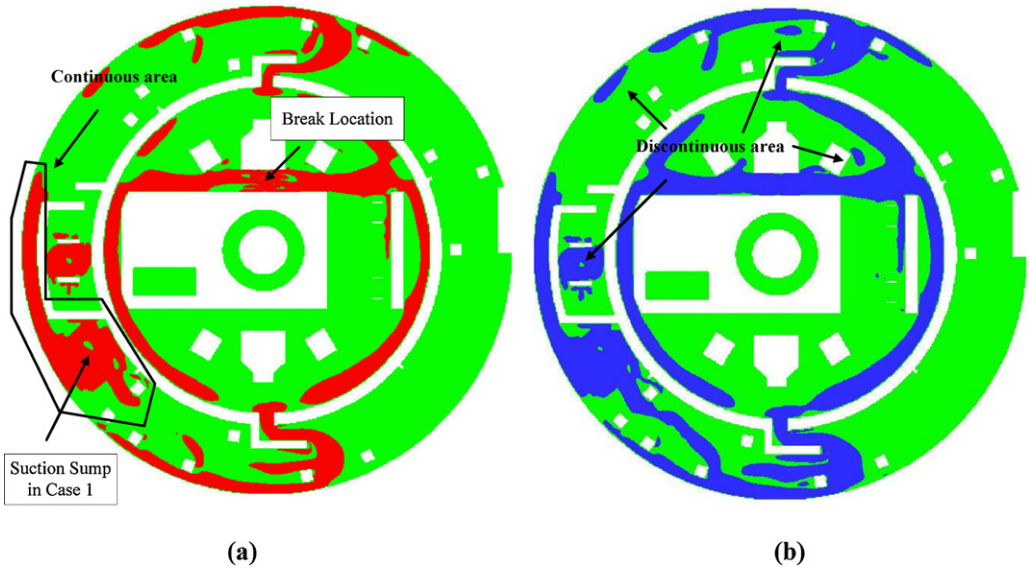

Fig. 21. Excess flow area of large NUKON based on (a) V_{mean} and (b) V_{max} profiles (Case 1).

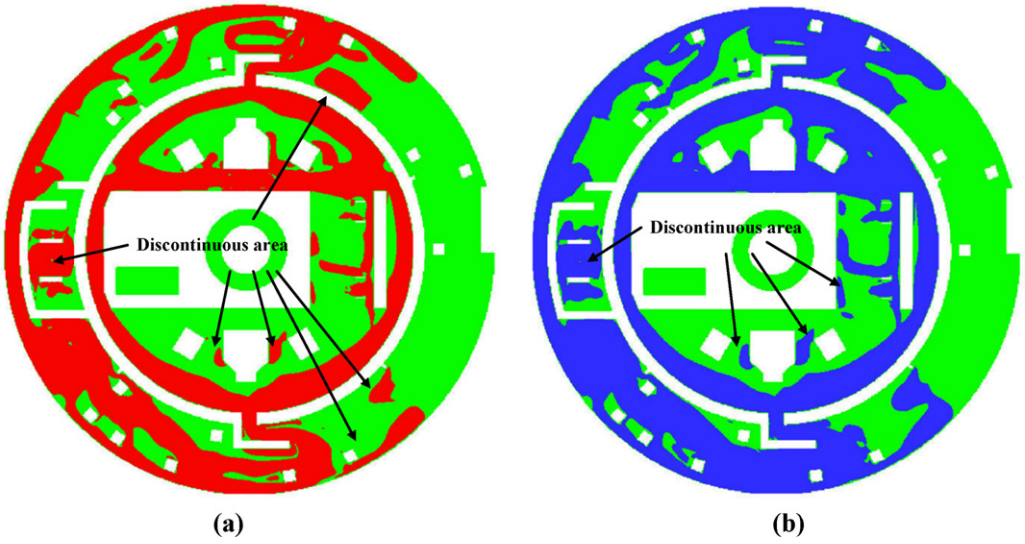

Fig. 22. Excess flow area of small/fine NUKON based on (a) V_{mean} and (b) V_{max} profiles (Case 1).

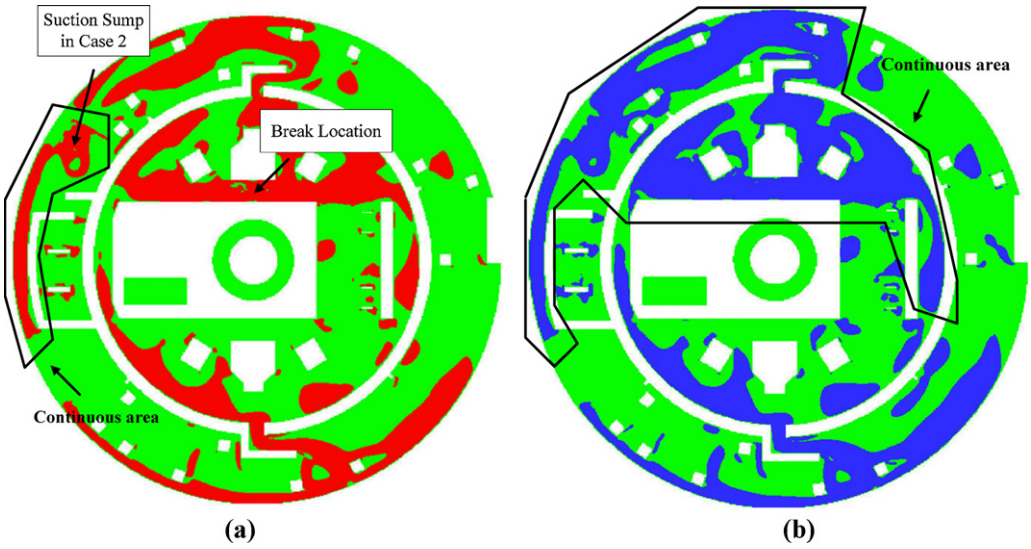

Fig. 23. Excess flow area of large NUKON based on (a) V_{mean} and (b) V_{max} profiles (Case 2).

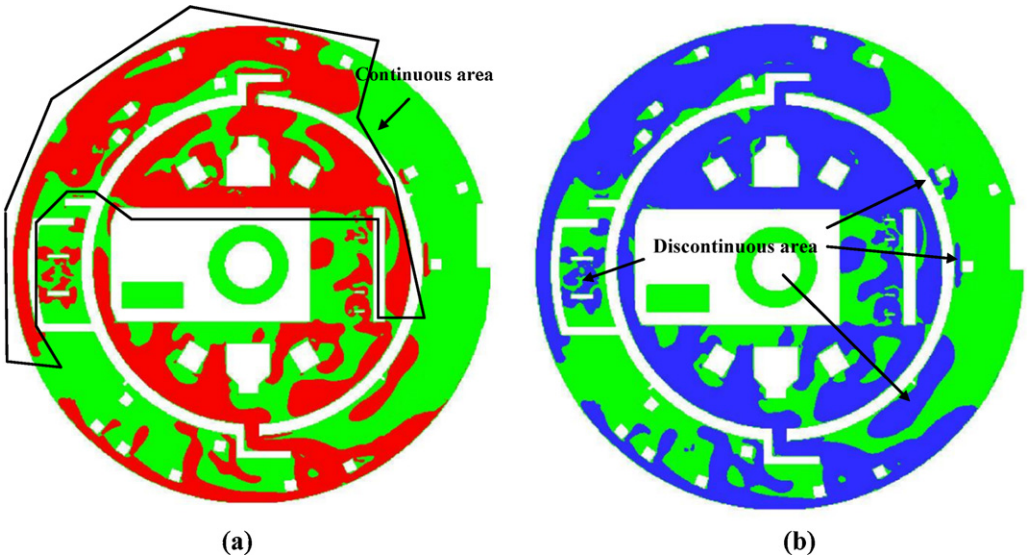

Fig. 24. Excess flow area of small/fine NUKON based on (a) V_{mean} and (b) V_{max} profiles (Case 2).

5. Conclusion

Through experiments and supplementary CFD analyses, it was shown that the effective tumbling velocity of debris augmented by the TKE can be represented by an algebraic sum of the mean horizontal velocity and the turbulence horizontal velocity deduced from the TKE. The debris transport fraction of OPR1000 was evaluated based on this finding and on a 3D CFD analysis. The results showed that a large increase in the debris transport is possible if the TKE is considered in the quantification process. Although there were some differences in the transport fraction depending on the debris size class, it was found that the debris transport fraction estimation may be increased by up to 5.55 times if the TKE effect is considered in the evaluation process using 3D CFD. This implies that the effect of TKE on debris transport augmentation should be considered if a conservative debris transport fraction is to be evaluated in resolving the GSI-191 safety issue.

The present study also shows that a conservative active sump location with respect to debris transport can vary depending on the debris size class. For instance, in spite of debris transport augmentation due to the TKE, a larger fraction of large NUKON debris was evaluated to be transported to a sump when a sump far from the break operates (Case 1) compared to the case when a sump near the break operates (Case 2). For small/fine NUKON, however, drastic TKE augmentation of debris occurs in Case 2 (2.06 times) compared to Case 1 (1.098 times). This implies that the location of the active sump also should be considered as an important parameter in a comprehensive debris transport evaluation considering maximum head loss at the sump screen.

Acknowledgements

This work was supported by the National Research Foundation of Korea (NRF) grant funded by the Korea Government (MEST) (Nos. 2009-0081824, 2010-0019543).

References

Bang, Y.S., Lee, G.S., Huh, B.G., Oh, D.Y., Woo, S.W., 2010. A particle tracking model to predict the debris transport on containment floor. Nucl. Eng. Technol. 42 (2), 211–218.

KHNP, 1998. Final Safety Analysis Report for ULCHIN Unit 3 & 4. Seoul.

Maji, A.K., Rao, D.V., Letrllier, B., Bartlein, L., Marshaal, B., 2002. Transport characteristics of selected pressurized water reactor LOCA generated debris. Nucl. Technol. 139, 145–155.

Maji, A.K., Letrllier, B., Ross, K.W., Rao, D.V., Bartlein, L., 2004. Experimental validation of CFD analyses for estimating the transport fraction of LOCA-generated insulation debris to ECCS sump screens. Nucl. Technol. 146, 279–289.

Nuclear Energy Institute, 2004. Pressurized Water Reactor Sump Performance Evaluation Methodology. NEI 04-07.

Park, J.Y., Kim, M.W., 2009. Study on new quantification methodology for pool recirculation debris transport in sump clogging issue. KINS/RR-688. Daejeon.

Park, J.P., Jeong, J.H., Kim, W.T., Kim, M.W., Park, J.Y., 2011. Debris transport evaluation during the blow-down phase of a LOCA using computational fluid dynamics. Nucl. Eng. Des. 241, 3244–3255.

USNRC, 1999. Drywell Debris Transport Study: Computational Work, NUREG/CR-6369, Vol. 3. Washington, DC.

USNRC, 2002a. GSI-191: Separate-Effects Characterization of Debris Transport in Water, NUREG/CR-6772. Washington, DC.

USNRC, 2002b. GSI-191: Integrated Debris Transport Tests in Water Using Simulated Containment Floor Geometries, NUREG/CR-6773. Washington, DC.

USNRC, 2003a. Regulatory Guide 1.82 Revision 3, Water Sources for Long-Term Recirculation Cooling Following a Loss-of-Coolant Accident. Washington, DC.

USNRC, 2003b. Knowledge Base for the Effect of Debris on Pressurized Water Reactor Emergency Core Cooling Sump Performance, NUREG/CR-6808. Washington, DC.

USNRC, 2004. Safety Evaluation by the Office of Nuclear Reactor Regulation Related to NRC Generic Letter 2004-02, Nuclear Energy Institute Guidance Report (Proposed Document Number NEI 04-07), Pressurized Water Reactor Sump Performance Evaluation Methodology. Washington, DC.

Ui, A., Kasahara, F., 2006. Development of a numerical method for flooding flow and transport of LOCA generated debris to sump screens. NTHAS5-I004. In: Proceedings of Fifth Korea-Japan Symposium on Nuclear Thermal Hydraulics and Safety, Korea, November 26–29.

Yakhot, A., Liu, H., Nikitin, N., 2006. Turbulent flow around a wall-mounted cube: a direct numerical simulation. Int. J. Heat Fluid Flow 27, 994–1009.

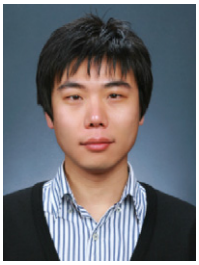

Jong Pil Park received his Master's degree from mechanical engineering at Pusan National University in 2008. He doing a Ph.D. His area of interest is thermal-hydraulic safety analysis and design in nuclear power plant using CFD code. He is currently working in CFD analysis of coolant flow in nuclear reactor vessel and discharged fluid behavior during LOCA based on CFD methodology.

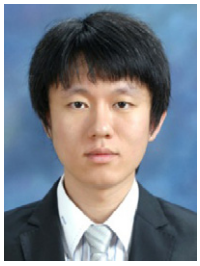

Kyung Sik Choi received his Master's degree from mechanical engineering at Pusan National University in 2011. Currently he works for Aritec Co., a nuclear engineering service company. His specialty is a thermal-hydraulic analysis of nuclear power plant.

Ji Hwan Jeong received his Ph.D. from the KAIST in 1995. He did his post-doctoral research in the Technology Centre in Aerodynamics and Heat Transfer at Oxford University. After three years of research experience at Korea Atomic Energy Research Institute, he joined the faculty of the school of mechanical engineering at Pusan National University. His research interests include multi-phase flow, nuclear safety, heat exchangers, heat pump, and computational fluid dynamics. He has also consulted in the nuclear and air conditioner industries.

Gyung-Min Choi received his Dr. Eng. from Osaka University in 2002. He worked as a researcher in the Japan Aerospace Exploration Agency until 2004. After three years of research experience, he joined the faculty of the school of mechanical engineering at Pusan National University. His research interests include combustion engineering, optical measurement and direct carbon fuel cell. He has also consulted in the gas turbine combustor and thermal power plant manufacturers.

Ju Yeop Park received a B.S. degree in Mechanical Engineering from Yonsei University in 1991. He then earned his M.S. and Ph.D. degrees from Korea Advanced Institute of Science and Technology in 1993 and 1999, respectively. Dr. Park is currently a Senior Researcher at Korea Institute of Nuclear Safety in Daejeon, Korea. His research interests are nuclear safety analysis, turbulence modeling and computational fluid dynamics.

Manwoong Kim has received his Ph.D. in mechanical engineering at University of Ottawa, Canada in 1996. He worked as a research associate at University of Ottawa. Since 1984, he had worked for Korea Atomic Energy Research Institute. From 1990, he was working for Korea Institute of Nuclear Safety in the field of thermal-hydraulic analysis. Currently, he is working for the International Atomic Energy Agency (IAEA) since 2009 as a safety officer and is responsible on safety assessment for nuclear installations. His research interests are addressed on multi-phase fluid flow, safety analysis and computational fluid dynamics for multi-components. Besides, he has lectured and consulted on the heat exchanger and HVAC design.